Cold collisions of Sr*-Sr in a magneto-optical trap

Timothy P. Dinneen, Kurt R. Vogel, Ennio Arimondo,* John L. Hall, and Alan Gallagher
JILA, National Institute of Standards and Technology, and University of Colorado, Boulder, Colorado 80309-0440
(Received 4 June 1998)

We present measurements of cold collision processes in an alkaline-earth species. Collisions of ^{88}Sr pairs in a magneto-optic trap are found to be dominated by very-long-range excitation to the nonradiating $^1\Pi_g$ state of Sr_2*. We find good agreement between measured loss rate coefficients and a modified form of the semiclassical model that includes retardation effects that allow excitation to metastable molecular states. [S1050-2947(99)00202-4]

PACS number(s): 34.50.Rk, 34.10.+x, 32.80.Pj

I. INTRODUCTION

Resonant absorption and spontaneous decay can dramatically affect the outcome of ultracold collisions and have inspired much theoretical interest in the study of cold collisions. These effects were observed in alkali-metal atom magneto-optic traps (MOTs), where they were found to limit both the trapping lifetime and the number of atoms that could be collected [1,2]. Atom traps have now become an important research tool in the study of ultralow-temperature atom-atom interactions. Precise photoassociative spectroscopy can be performed at these temperatures that can be used for extracting *s*-wave scattering lengths [3], precise atomic lifetimes [4,5], and investigating long-range molecular structure [6–8].

In a MOT, excited atoms interact with ground-state atoms via the long-range R^{-3} resonant dipole interaction, which leads to two different loss mechanisms for these ultracold atoms. The first is state-changing collisions occurring at a small internuclear distance; atoms that change state and leave on a lower molecular potential gain sufficient kinetic energy to be ejected from the trap. The second is radiative escape: An excited pair of atoms spontaneously decays at a small internuclear distance and the kinetic energy gained from the R^{-3} potential can be large enough to cause trap loss. The rates for both loss processes depend critically on molecular radiative lifetimes because the initial kinetic energy of the atom pair is so small that the collision duration can be much greater than the spontaneous decay time.

A simple semiclassical model for collisional loss was introduced by Gallagher and Pritchard in 1989 [9]. This model involved excitation of the atom pair to the R^{-3} potential at large distances ($\sim$500 Å) and calculation of a survival probability along a classical trajectory to small distances where radiative escape or a state-changing collision could occur. The model assumed the initial kinetic energy of the atoms to be negligible in comparison to the potential energy at excitation and assumed a single attractive molecular potential for the collision. In dealing with the alkali-metal atoms, this single potential approach is quite an oversimplification of the complex dimer potentials due to fine and hyperfine structure. Julienne and Vigue (JV) improved on the model to include collisions on multiple attractive potentials and introduced a temperature dependence to provide a more general theory with a link to room-temperature experiments [10,11]. JV predicted the importance of metastable molecular states to fine-structure changing collisions in the heavy alkali-metal atoms, but the model still ignored the hyperfine structure.

A comparison of trap loss experiments with the semiclassical theories shows qualitative agreement and estimates of the importance of various molecular potentials to trap loss can be made [14–18]. These experiments infer that long-lived molecular states must be included to describe alkali-metal trap loss, but hyperfine mixing of these states prevents quantitative comparisons with theory. Experiments become more quantitative when excitation is made to specific states beyond the range of the hyperfine structure and specific collision channels can be isolated [19].

Cold atoms interact at distances where the R^{-3} potential is small compared to the hyperfine structure in the alkali-metal atoms and the coupling of many levels occurs during a collision [12]. If the complications that the hyperfine structure introduces to the collision dynamics can be avoided, it should be possible to make quantitative predictions for cold collision processes. Alkaline-earth atoms provide an ideal system for the study of these processes since the even isotopes have no hyperfine structure and can be laser cooled on their strong $^1S_0 \rightarrow {}^1P_1$ cycling transition. The resonant $^1S \rightarrow {}^1P$ interaction has no fine structure and yields only four molecular potentials, proportional to R^{-3}, two of which are repulsive and two attractive. The two attractive potentials lead to trap loss collisions and of these the $^1\Pi_g$ state is a long-lived nonradiating state while the $^1\Sigma_u^+$ state radiates at twice the atomic rate. The simplicity of the long-range interactions makes these atoms ideal candidates for testing cold collision theories.

II. SEMICLASSICAL THEORY

The two attractive potentials of the Sr dimer are $-C_{\Pi,\Sigma}R^{-3}$, where $C_\Pi = 10$ a.u. and $C_\Sigma = 20$ a.u. The $^1\Sigma_u^+$ state radiates at twice the atomic rate but the gerade symmetry of the $^1\Pi_g$ state prevents decay to the ground state. Since the $^1\Sigma_u^+$ state has a lifetime of only 2.5 ns, survival of the excited pair to small interatomic distance is very unlikely.

*Permanent address: Dipartimento di Fisica, Università di Pisa, Piazza Torricelli 2, I-56126, Pisa Italy.

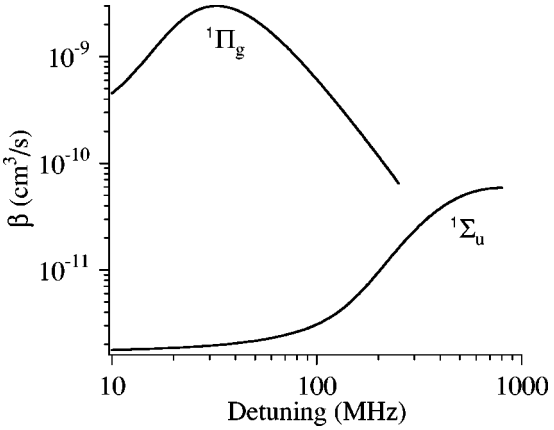

FIG. 1. Trap loss rate coefficients from Appendix A for excitation to the $^1\Pi_g$ metastable molecular state along with the standard GP result for excitation to the strong decaying $^1\Sigma_u^+$ state. The total trap loss rate is βn, where n is the trap density. The results are shown for an excitation intensity of 60 mW/cm^2.

However, for the $^1\Pi_g$ state, retardation effects at large internuclear distances mix the two states allowing strong excitation to the $^1\Pi_g$ state, which then becomes metastable as the collision proceeds. We measure a large trap loss rate that confirms the importance of this long-lived $^1\Pi_g$ state in the trap loss process.

From Meath [20], the linewidth of the $^1\Pi_g$ molecular state as a function of the internuclear separation is given by

$$\Gamma_{\Pi}=\frac{\Gamma_a}{5}\left(\frac{R}{\lambda\!\!\!^{-}}\right)^2 \quad \text{with} \quad R<\lambda\!\!\!^{-}, \tag{1}$$

where Γ_a and $\lambda\!\!\!^{-}$ are the atomic decay rate and wavelength, respectively. This radial dependence has a tremendous impact on the excitation rate and survival probability of a long-range pair in the Gallagher-Pritchard (GP) model. The $^1\Pi_g$ state very efficiently induces trap loss because it can absorb at large R, but it radiates weakly at small R, enhancing the survival probability during transit to $R<10$ Å, where state changing collisions can occur [13]. A comparison of the survival probability for the two states demonstrates this effect. From Appendix A the probability of survival for the $^1\Pi_g$ state, expressed in terms of the laser detuning δ, is

$$S(^1\Pi_g)=e^{-(\delta_s/\delta)^{3/2}}, \tag{2}$$

with $\delta_s=43$ MHz. In comparison, the survival probability for the $^1\Sigma_u$ state is

$$S(^1\Sigma_u)=e^{-(\delta_s/\delta)^{5/6}}, \tag{3}$$

where now $\delta_s=2.2$ GHz.

Figure 1 shows the two-body cold collision loss rate coefficient β as a function of laser detuning for the $^1\Pi_g$ and $^1\Sigma_u$ states. Typical trap detunings used in the experiment are 40–60 MHz, where the $^1\Pi_g$ state clearly plays the dominant role. At these detunings the loss rate due to the $^1\Sigma_u$ state comes entirely from absorption at small internuclear separation in the Lorentzian wings of the transition. Approximations in our semiclassical theory include zero initial kinetic energy for the atom pair and unit probability for state-changing collisions if the pair survives to a small distance.

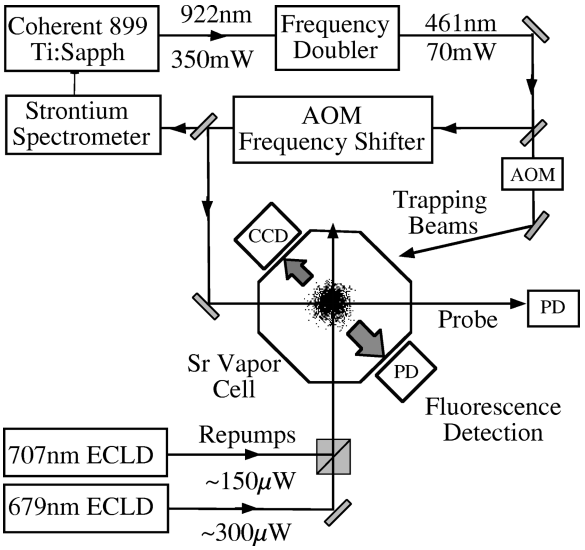

FIG. 2. Schematic of the experimental setup showing the Ti:sapphire trapping laser, the extended cavity laser diodes (ECLD's) for repumping at 679 and 707 nm, and detection photodiodes (PD's).

III. EXPERIMENTAL APPARATUS

An outline of the experimental apparatus is shown in Fig. 2; a more detailed description can be found in Ref. [21]. The experiment consists of a Sr vapor cell MOT using the $^1S_0 \rightarrow {}^1P_1$ cycling transition at 461 nm to laser cool and trap. The vapor cell is machined from a solid block of polycrystalline alumina to which sapphire windows are attached. It operates between 250 °C and 350 °C providing vapor densities in the range $\sim 10^6-10^8$ cm^{-3}. The output of a Coherent 899 Ti:sapphire laser [22] at 922 nm is frequency doubled to make 70 mW of 461-nm light. The Ti:sapphire laser is offset locked to the ^{88}Sr resonance center in a saturation spectrometer via a double-pass acousto-optic modulator (AOM) that allows accurate control over the trap detuning. Another AOM is used to stabilize the trap light intensity and a mechanical shutter is used to switch the trap light. The MOT itself is a standard six beam σ_+-σ_- configuration used in conjunction with a 70-G/cm quadrupole field. At maximum laser power we achieve a total MOT laser intensity of 60 mW/cm^2 in 1-cm-diam beams ($1/e^2$) and can capture 5×10^6 atoms in steady state from a background density of 5×10^8 cm^{-3}. This maximum number is achieved with a laser detuning of -56 MHz and produces a trap of 0.6 mm($1/e$) radius.

The cooling transition is not completely closed, as can be seen in Fig. 3. A small leak to the low-lying $^1D_2$ state is fed by the $^1P_1$ excited state with a branching ratio of 2×10^{-5}, which is small enough that most trapped atoms have reached a steady-state velocity before decaying to the $^1D_2$ state. The $^1D_2$ state ($\tau=0.3$ ms) further decays to the $^3P_{1,2}$ states, but only $^3P_1$ ($\tau=21$ μs) returns the atom to the cycling transition. The MOT lifetime is thus determined by the loss to the $^3P_2$ metastable level. We calculate this shelving loss as $\Gamma_s=f\gamma_{P-D}\mathcal{L}$, where f is the $^1P_1$ excited fraction,

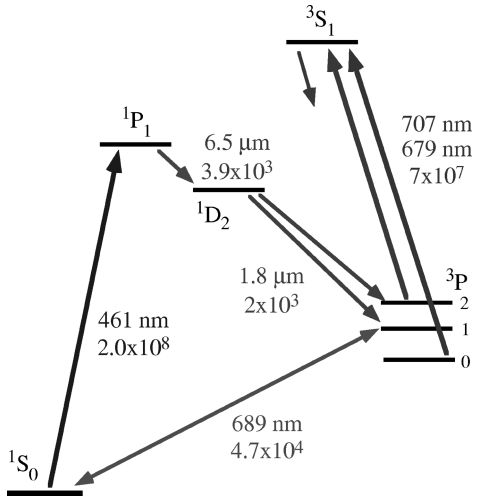

FIG. 3. Level diagram for strontium showing important transition wavelengths and decay rates for the operation of the MOT.

γ_{P-D} is the decay rate $^1P_1 \rightarrow {}^1D_2$, and $\mathcal{L}$ is the branching ratio to the $^3P_2$ state. With an excited fraction $f \sim 5\%$, $\gamma_{P-D} = 3900\ \mathrm{s}^{-1}$ [23], and $\mathcal{L} = 0.3$ [24], we have $\Gamma_s^{-1} = 17$ ms, in excellent agreement with the observed lifetime. For comparison, the calculated loss rate due to background Sr atoms at this temperature is less than $1\ \mathrm{s}^{-1}$.

To eliminate the shelving loss mechanism we optically pump to the short-lived $^3S_1$ state ($\tau = 16$ ns), which returns atoms to the ground state via the $^3P_1$ state. Diode lasers at 679 and 707 nm were used to repump the $^3P_{0,2}$ levels, respectively. Each of these lasers was side locked to a fringe of a stable Zerodur reference cavity to reduce drift rates to less than 20 MHz/h. With both repump lasers in operation we found a factor of 10 improvement in the number of trapped atoms and a corresponding reduction in the loss rate. However, for our background density of $3 \times 10^8\ \mathrm{cm}^{-3}$, in the absence of two-body trap loss collisions, we would have expected a 100-fold improvement in trap lifetime to greater than 1 s. Changing the density of the trap reveals a density-dependent loss rate characteristic of cold two-body collisions.

IV. RESULTS

The density of atoms in the trap is governed by the trap loading equation

$$\dot{n} = L_n - \Gamma n - \beta n^2, \tag{4}$$

where n is the density, L_n the loading rate, Γ the linear loss rate, and β the coefficient for two-body collisional loss. The solution to this equation is

$$n = n_{ss}\left(\frac{1 - e^{-\gamma t}}{1 + \xi e^{-\gamma t}}\right), \tag{5}$$

where n_{ss} is the steady-state density and

$$\gamma = \Gamma + 2\beta n_{ss}, \tag{6}$$

$$\xi = \beta n_{ss}/(\beta n_{ss} + \Gamma) \tag{7}$$

represent the total trap loss rate and cold collision fraction, respectively. When linear losses dominate, the ξ parameter of Eq. (7) goes to zero and Eq. (5) becomes exponential, as is the case for the shelving loss. In the presence of the repumping lasers the shelving loss is essentially eliminated and the trap loading curves become nonexponential. The total number of atoms in the trap as a function of time is measured through the fluorescence signal and the density-dependent loading equation must be integrated over the trap volume. The loading equation (4) becomes

$$\dot{N} = L_N - \Gamma N - \beta \int n^2(\mathbf{r})\, d^3\mathbf{r} \tag{8}$$

and we need to characterize the trap density distribution in order to extract the two-body loss rate coefficient from the fluorescence measurements.

The density is measured using absorption of a 461-nm probe in parallel with measurements of the trap distribution using a charge-coupled device (CCD) camera. The trap has a Gaussian distribution except at the highest numbers ($>10^7$) where distortions begin to appear, in contrast to the alkali-metal atom traps, where the deviation from a Gaussian distribution begins with as few as 5×10^4 atoms [2]. The modification of the density is due to radiation trapping, which is the reabsorption of photons emitted from the trapped atoms, and occurs when the optical depth exceeds unity. Most alkali-metal traps operate with an optical depth much greater than unity and the density distribution becomes almost uniform. In the case of the alkaline-earth atoms the absence of sub-Doppler cooling results in much higher trap temperatures. These hotter atoms occupy a much larger volume and the optical depth does not reach the critical value until there are more than 10^7 atoms in the trap. With a typical $1/e$ trap radius of 0.6 mm the resulting radiation trapping density threshold is $\sim 10^{10}\ \mathrm{cm}^{-3}$.

In this constant volume regime $n = n_0 e^{-(r/a)^2}$ and Eq. (8) becomes

$$\dot{N} = L_N - \Gamma N - \beta' N^2, \tag{9}$$

with $\beta' = \beta(\sqrt{2\pi}\, a)^{-3}$ and a solution of the form of Eq. (5). The loss rate parameter (6) becomes

$$\gamma = \Gamma + 2\beta' N_{ss} = \Gamma + \beta n_0/\sqrt{2} \tag{10}$$

and the collision loss fraction becomes

$$\xi = \frac{\beta n_0}{\beta n_0 + 2\sqrt{2}\Gamma}, \tag{11}$$

where $N_{ss} = n_0(\sqrt{\pi}a)^3$ is the steady-state number. The second equality in Eq. (10) is very useful as it relates the loss rate γ, extracted directly from the fluorescence loading curve, to the peak trap density n_0, which can be measured through absorption. A typical nonexponential loading curve is shown in Fig. 4 along with a fit to the form of Eq. (5).

This fit produces results for the trap loss rate γ to a precision of about 1% and results for the ξ parameter that are good to 25%. A large uncertainty is not unexpected here because the ξ parameter is essentially a correction term to an

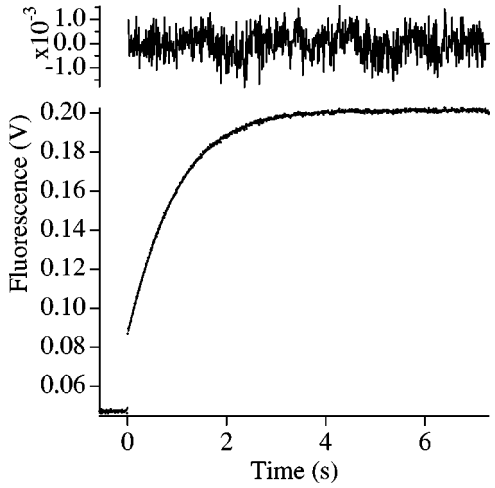

FIG. 4. Typical fluorescence loading curve for the trap shown in the lower trace for trap detuning of -40 MHz, trap intensity $I=1.4I_{sat}$, and trap density $n=2\times10^{9}$ cm^{-3}. The fit is indistinguishable from the data, as seen by the fit residuals in the upper trace.

exponential curve and is sensitive to low-frequency fluctuations in the data. Despite efforts to stabilize the intensity of the trap light, air currents produced by the hot cell resulted in beam instability that contributed to low-frequency trap signal variations at the 1% level creating the uncertainty in ξ. A simple exponential fit to the data results in systematic residuals at the level of 3%, indicating the need for the ξ term. Since the collision information is strongly encoded in the well determined γ parameter, a series of fluorescence loading curves was taken as a function of trap density to better extract the collision term and also search for systematic effects. The results for γ are plot as a function of density and used to extract Γ and β. A plot of γ and ξ versus density can be seen in Fig. 5.

Equations (6) and (7) predict that the loss rate γ should vary linearly with density while ξ should saturate to a value of 1. However, as can be seen in Fig. 5, when the density increases beyond 1×10^{10} cm^{-3} the ξ parameter returns to zero, indicating a transition from the constant volume regime to a constant density regime. This signature of the onset of radiation trapping is in agreement with optical depth measurements and is confirmed by direct measurement of the trap size, which show that it remains constant to within 4% for densities less than 1×10^{10} cm^{-3} but expands thereafter. Our analysis, based on Eq. (9), assumes a constant volume operation for our trap and we cannot expect to extract reliable values for the loss rate above 1×10^{10} cm^{-3}. We therefore restrict the density range in our analysis to data taken below this value.

A plot of γ versus peak density n_0 for this restricted range is shown in Fig. 6. Fitting Eq. (10) to the data gives $\Gamma=0.68(5)$ s^{-1} and $\beta=4.5(0.3)(1.1)\times10^{-10}$ cm^3 s^{-1}. The 7% statistical error in β is due to uncertainty in relative density caused by uncertainty in the trap size measurements. The dominant 25% systematic error in β is due to the uncertainty in the absolute density calibration. The residual linear loss term $\Gamma=0.68(5)$ s^{-1} appears to be due to incomplete optical pumping of the shelved atoms and is sensitive to the magnetic field gradient, trap beam detuning, alignment, and

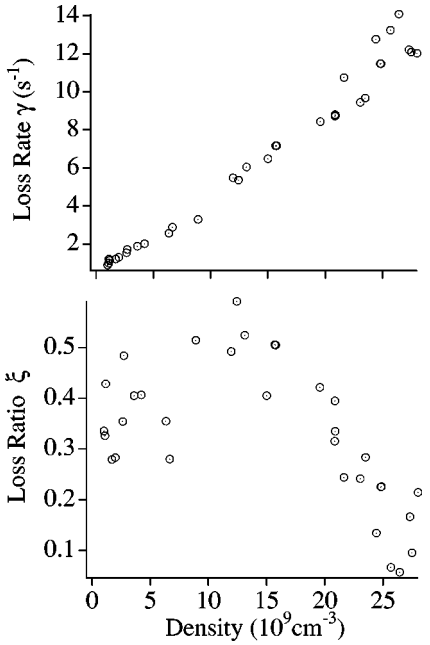

FIG. 5. (a) Plot of the total loss rate γ versus peak density n_0 at a trap detuning of -40 MHz and trap beam intensity of 60 mW/cm^2. (b) Corresponding loss ratio ξ. In the absence of radiation trapping ξ should saturate to a value of 1. Although the data are poor, it is clear that ξ returns to zero instead of saturating.

size, as well as the repump power. To ensure that this term remained constant during a measurement run, the density was varied by changing the operating temperature of the cell. The loss rate due to background strontium atoms does depend on the temperature of the cell but is estimated to be less than 0.03 s^{-1} for all the data shown in Fig. 6.

From Appendix A, the theoretical results for atoms with zero initial kinetic energy give loss rate coefficients of 2.0×10^{-12} and 2.5×10^{-9} cm^3 s^{-1} for the $^1\Sigma_u$ and $^1\Pi_g$ states, respectively. The theoretical result assumes complete loss of the pair if it survives to $R<10$ Å and does not take into account details of the state-changing mechanism or the multiple vibrations that can occur due to the large survival probability in the case of the $^1\Pi_g$ state. However, there are sev-

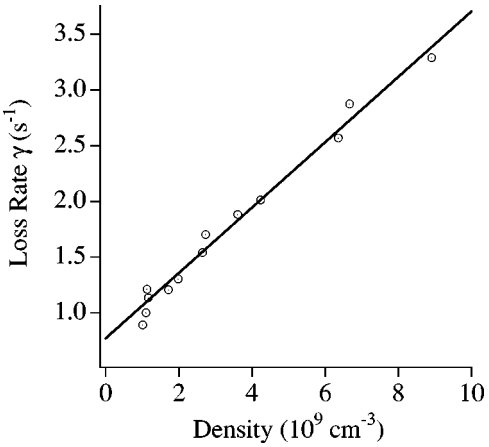

FIG. 6. Plot of the total loss rate γ versus peak density n_0 at a trap detuning of -40 MHz and trap beam intensity of 60 mW/cm^2. The fit gives $\beta=4.5\times10^{-10}$ cm^3 s^{-1} and $\Gamma=0.68$ s^{-1}.

eral states below the atomic $^1P_1$ state that contribute to level crossings below 10 Å in the molecule, which implies that there are many chances for a loss process to occur by the time the atoms reach $R=0$.

Finite temperatures alter the collision trajectories and we make an estimate of the temperature corrections to the survival of the $^1\Pi_g$ state in Appendix B. For temperatures at the Doppler limit the survival factor is reduced to 0.75 of the stationary value. However, temperatures measured in our trap are generally hotter than the Doppler limit, reducing the loss rate coefficient to 0.5 of the stationary value. Saturation of the narrow $^1\Pi_g$ state is also a concern, but the line is broadened by free-bound Franck-Condon factors. The spectral width of the state due to this effect is estimated to be ~ 30 MHz, while the natural linewidth is 4.5 MHz. At the trap operating intensity of 60 mW/cm^2 we estimate a reduction of the loss rate coefficient by only 20% due to saturation. Combining these factors the best theoretical estimate for the loss rate coefficient in our trap becomes 1.0×10^{-9} cm^3 s^{-1} compared with the measured value of $4.5(0.3)(1.1)\times 10^{-10}$ cm^3 s^{-1}.

V. CONCLUSION

In summary, we have presented trap loss measurements in an alkaline-earth system. In this system, free of fine and hyperfine structures, the molecular states simplify to just two collision channels of very different character. We compare the experimental results with a semiclassical GP model that describes excitation to both the short-lived $^1\Sigma_u$ and long-lived $^1\Pi_g$ molecular states. Despite its limitations, the semiclassical theory provides good agreement with the experimental results and clearly demonstrates the importance of long-lived molecular states for trap loss collisions. This is in contrast to the alkali-metal systems where the semiclassical calculations are limited to an order of magnitude due to the hyperfine effects. For more accurate comparisons with experiment a fully quantum treatment that deals with the details of the state changing mechanism is more appropriate.

ACKNOWLEDGMENTS

The authors thank Marla Dowell and Alex Olivas for their assistance in the initial stages of this experiment and Hans Green for construction of the ceramic vapor cell. We would also like to acknowledge John Bohn for his insightful theoretical discussions on atomic collisions. Finally, we thank Carl Wieman and Eric Cornell for generous equipment loans. This work has been supported by the NSF and NIST.

APPENDIX A: SUMMARY OF SEMICLASSICAL MODEL FOR TRAP LOSS

The two-body loss rate from the trap is found by calculating

$$R_{loss}=2\int d^3(\mathbf{r})\left(\frac{1}{2}\beta n^2(\mathbf{r})\right), \tag{A1}$$

where β is the rate coefficient for two body loss, $n(\mathbf{r})$ is the atom density distribution, the factor of 1/2 corrects for double counting, and the factor 2 accounts for the two particles removed in each collision. The rate coefficient β is calculated by integrating the excitation and survival rates over the atom pair distribution

$$\beta=\int_0^\infty dR_0\, 4\pi R_0^2\left(\frac{I\sigma(R_0)}{\hbar\omega_L}\right)S(R_0). \tag{A2}$$

The $4\pi R_0^2$ term gives the number distribution at a distance R_0 from our target atom, $I\sigma(R_0)/h\omega_L$ is the excitation rate at separation R_0, and $S(R_0)$ is the probability of the atom pair surviving in the excited state until colliding at $R\sim 0$.

The absorption rate is given by

$$\frac{I\sigma(R_0)}{\hbar\omega_L}=\frac{I}{\hbar\omega_L}\frac{\lambda^2}{2\pi}\left[\frac{[\Gamma_m(R_0)/2]^2}{[\Gamma_m(R_0)/2]^2+\Delta(R_0)^2}\right], \tag{A3}$$

where $\Delta(R_0)=\omega_0-\omega_L-C_3R_0^{-3}/\hbar$ is the detuning from the molecular resonance, $\Gamma_m(R_0)$ is the molecular decay rate for separation R_0, and ω_L and I are the laser excitation frequency and intensity. The survival factor $S(R_0)$ is written

$$S(R_0)=\exp\left(-\int_0^{t_c}\Gamma_m(t)dt\right), \tag{A4}$$

where t_c is the time to collision. From the classical equations of motion we can convert the time integral to a position integral. Assuming zero initial kinetic energy of the pair we have

$$\frac{1}{2}\mu\dot{R}^2=C_3(R^{-3}-R_0^{-3}), \tag{A5}$$

where μ is the reduced mass of the colliding pair. We can then write

$$dt=dR\sqrt{\frac{\mu R_0^3}{2C_3}}[(R_0/R)^3-1]^{-1/2} \tag{A6}$$

and the survival factor becomes, with $x=R/R_0$,

$$S(R_0)=\exp\left(-\sqrt{\frac{\mu R_0^5}{2C_3}}\int_0^1\frac{\Gamma_m(x)\,dx}{\sqrt{x^{-3}-1}}\right). \tag{A7}$$

Setting the lower integration limit to zero introduces a negligible error in the calculation and if we set $\Gamma_m(R)=2\Gamma_a$ as is appropriate for the $^1\Sigma_u$ state we obtain the results of the semiclassical (GP) model. The integral in Eq. (A7) simplifies to $\int_0^1 dx/\sqrt{x^{-3}-1}=0.747$ and using $C_3=1.27\times 10^{-47}$ J/m^3 the survival factor can be written

$$S(R_0)=\exp-(R_0/R_s)^{5/2}=\exp-(\delta_s/\delta)^{5/6}, \tag{A8}$$

where $R_s=206$ Å and $\delta_s=2.2$ GHz. Combining Eqs. (A8), (A3), and (A2) and expressing the integral in terms of the detuning δ we can write

$$\beta(\delta_L,I)=2.9\times10^{-8}I\int_0^\infty dx\,\frac{x^{-2}\exp(-x^{-5/6})}{1+a^2(x-\delta_L/\delta_s)^2},\quad\text{(A9)}$$

where I is the trap intensity in W/cm^2, $x=\delta/\delta_s$, $a=2\pi\delta_s/\Gamma_a=68$, $2\pi\delta_L=(\omega_0-\omega_L)$ is the laser detuning from the atomic resonance, and β is in units of cm^3/s.

For the metastable $^1\Pi_g$ state Meath gives

$$\frac{\Gamma_\Pi}{\Gamma_a}=1-\frac{3}{2}y^{-3}[(y^2-1)\sin y+y\cos y],\quad\text{(A10)}$$

where $y=R/\lambda\!\!\!^{-}$ and Γ_a is the atomic decay rate. For $R<\lambda\!\!\!^{-}$ this expression can be simplified to

$$\Gamma_m=\frac{\Gamma_a}{5}\left(\frac{R}{\lambda\!\!\!^{-}}\right)^2,\quad\text{(A11)}$$

accurate to 5% at $R=\lambda\!\!\!^{-}$. At typical trap detunings our excitation radius R (400–600 Å) is less than $\lambda\!\!\!^{-}$ and we use the simpler expression to write the survival factor (A7) as

$$S(R_0)=\exp\left(-\frac{\Gamma_a}{5\lambda\!\!\!^{-2}}\sqrt{\frac{\mu R_0^9}{2C_3}}\int_0^1\frac{dx\,x^2}{\sqrt{x^{-3}-1}}\right).\quad\text{(A12)}$$

Using $C_3=6.35\times10^{-48}$ J/m^3 for the $^1\Pi_g$ state, with $\int_0^1 dx\,x^2/\sqrt{x^{-3}-1}=\pi/6$ we can write

$$S(R_0)=\exp[-(R_0/R_s)^{9/2}]=\exp[-(\delta_s/\delta)^{3/2}],\quad\text{(A13)}$$

where $R_s=610$ Å and $\delta_s=43$ MHz. Combining Eqs. (A13), (A3), and (A2) and writing the integral in terms of the detuning we find

$$\beta(\delta_L,I)=7.3\times10^{-7}I_r\int_0^\infty dx\,\frac{x^{-2}\exp(-x^{-3/2})}{1+a(x-\delta_L/\delta_s)^2x^{4/3}},\quad\text{(A14)}$$

where I is the trap intensity in W/cm^2, $x=\delta/\delta_s$, $a=(5\lambda^2/\pi\Gamma_a)^2\delta_s^{10/3}(h/C_3)^{4/3}=377$, δ_L is the laser detuning from the atomic resonance, and β is in units of cm^3/s. The results of this integration are shown in Fig. 1.

APPENDIX B: TEMPERATURE CORRECTIONS

So far the theory assumes that two atoms, initially at rest, fall directly to $R=0$ along the excited potential. However, finite temperatures cause the atoms to follow curved trajectories, some of which never reach $R=0$ and cannot cause trap loss. A correction to the semiclassical model can be made as follows. For an atom pair excited at radius R_0 with initial relative velocity $\vec{v}_r=\vec{v}_1-\vec{v}_2$ and angular momentum $L=\mu\vec{R}_0\times\vec{v}_r=\mu v_r R_0\sin\theta_0$, the conservation of energy gives

$$\frac{1}{2}\mu\dot{R}^2+\frac{L^2}{2\mu R^2}-C_3R^{-3}=\frac{1}{2}\mu v_r^2-C_3R_0^{-3},\quad\text{(B1)}$$

which can be rewritten as

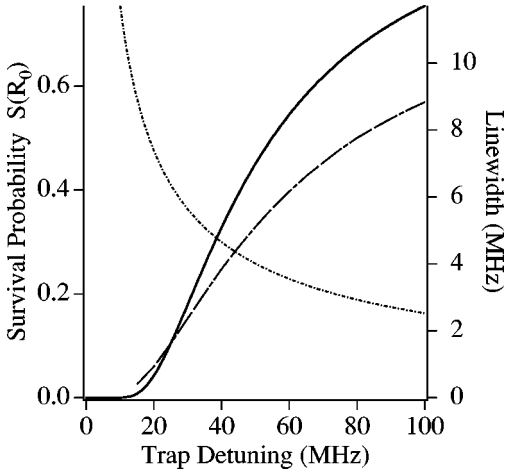

FIG. 7. Survival factor $S(R)$ for zero initial kinetic energy (solid line) and temperatures at the Doppler limit (dashed line). Over the range 40–100 MHz the Doppler limit survival factor is reduced to 0.75 of the zero-kinetic-energy value. Also shown is the natural linewidth of the $^1\Pi_g$ state (dotted line).

$$\dot{R}^2=v_r^2\left(1-\frac{R_0^2}{R^2}\sin^2\theta_0\right)+\frac{2C_3R_0^{-3}}{\mu}\left(\frac{R_0^3}{R^3}-1\right),\quad\text{(B2)}$$

and Eq. (A6) becomes

$$dt=\pm dR\sqrt{\frac{\mu R_0^3}{2C_3}}[f(1-g(R_0/R)^2)+(R_0/R)^3-1]^{-1/2},\quad\text{(B3)}$$

where $f=\mu v_r^2/2C_3R_0^{-3}$ is the ratio of initial kinetic energy to potential energy, $g=\sin^2\theta_0$ is an initial impact angle, and the sign distinguishes atoms initially moving together or apart.

For the inbound atoms ($\theta_0<\pi/2$) the general survival factor (A7) becomes

$$S(R_0)=\exp\left(-\sqrt{\frac{\mu R_0^5}{2C_3}}\int_0^1\frac{\Gamma_m(x)\,dx}{\sqrt{f(1-gx^{-2})+x^{-3}-1}}\right).\quad\text{(B4)}$$

For $\theta_0>\pi/2$, an additional integration is performed from $x=1\to x_m$ and back, where x_m is the outer turning point. Not all trajectories result in $R\to0$, which places constraints on $g=\sin\theta$ when integrating over the velocity distribution. The normalized velocity distribution is given by

$$N(v,dv,\theta,d\theta)=\frac{2}{\sqrt{\pi}}\sin\theta\,d\theta\,dy\,y^2e^{-y^2},\quad\text{(B5)}$$

where $y=v/v_0$ and v_0 is the most probable speed.

For atoms cooled to the Doppler limit we have

$$k_BT_D=\frac{\hbar\Gamma_a}{2}\left(\frac{1+(\delta_L/\gamma_a)^2}{2\delta_L/\gamma_a}\right),\quad\text{(B6)}$$

where k_B the Boltzmann constant, δ_L is the laser detuning, and $\gamma_a=\Gamma_a/4\pi$ is half-width of the atomic transition. Introducing $f=f_0y^2$ and noting that $v_0^2=\frac{2}{3}v_{rms}^2$ we can write

$$f_0 = \frac{mv_0^2}{2C_3R_0^{-3}} = \frac{k_B T_D}{h\delta_L} = \left(\frac{1+(\delta_L/\gamma_a)^2}{2(\delta_L/\gamma_a)^2} \right). \quad \text{(B7)}$$

For $\delta_L > 2\gamma_a$, f_0 is essentially constant and the survival factor (B4) scales uniformly with detuning. The results of the integration are shown in Fig. 7.

Temperature measurements performed at a detuning of 56 MHz indicate an intensity dependence for the temperature. At an intensity of 60 mW/cm^2 the trap temperature is twice the Doppler limit. At this temperature the survival factor is reduced to 50% of the zero-temperature result at 56 MHz. Temperature measurements at other detunings are still under investigation.

[1] E. L. Raab, M. G. Prentiss, A. E. Cable, S. Chu, and D. E. Pritchard, Phys. Rev. Lett. **59**, 2631 (1987).

[2] D. Sesko, T. Walker, C. Monroe, A. Gallagher, and C. Wieman, Phys. Rev. Lett. **63**, 961 (1989).

[3] R. Napolitano, J. Weiner, C. J. Williams, and P. S. Julienne, Phys. Rev. Lett. **73**, 1352 (1994).

[4] K. M. Jones, P. S. Julienne, P. D. Lett, W. D. Phillips, E. Tiesinga, and C. J. Williams, Europhys. Lett. **35**, 85 (1996).

[5] W. I. McAlexander, E. R. I. Abraham, and R. G. Hulet, Phys. Rev. A **54**, R5 (1996).

[6] H. R. Thorsheim, J. Weiner, and P. S. Julienne, Phys. Rev. Lett. **58**, 2420 (1987).

[7] John Weiner, J. Opt. Soc. Am. B **6**, 2270 (1989).

[8] P. L. Gould, P. D. Lett, P. S. Julienne, W. D. Phillips, H. R. Thorsheim, and J. Weiner, Phys. Rev. Lett. **60**, 788 (1988).

[9] A. Gallagher and D. E. Pritchard, Phys. Rev. Lett. **63**, 957 (1989).

[10] P. S. Julienne and Jacques Vigue, Phys. Rev. A **44**, 4464 (1991).

[11] P. S. Julienne, A. M. Smith, and K. Burnett, Adv. At., Mol., Opt. Phys. **30**, 141 (1993).

[12] Carl J. Williams and Paul S. Julienne, J. Chem. Phys. **101**, 2634 (1994).

[13] N. Boutassetta, A. R. Allouche, and M. Aubert-Frécon, Phys. Rev. A **53**, 3845 (1996).

[14] C. D. Wallace, T. P. Dinneen, K. Y. N. Tan, T. T. Grove, and P. L. Gould, Phys. Rev. Lett. **69**, 897 (1992).

[15] L. Marcassa, V. Bagnato, Y. Wang, C. Tsao, J. Weiner, O. Dulieu, Y. B. Band, and P. S. Julienne, Phys. Rev. A **47**, R4563 (1993).

[16] P. D. Lett, K. Mölmer, S. D. Gensemer, K. Y. N. Tan, A. Kumarakrishnan, C. D. Wallace, and P. L. Gould, J. Phys. B **28**, 65 (1995).

[17] T. Walker and P. Feng, Adv. At., Mol., Opt. Phys. **34**, 125 (1994).

[18] S. D. Gensemer and P. L. Gould, Phys. Rev. Lett. **80**, 936 (1998).

[19] M. G. Peters, D. Hoffmann, J. D. Tobiason, and T. Walker, Phys. Rev. A **50**, R906 (1994).

[20] William J. Meath, J. Chem. Phys. **48**, 227 (1968).

[21] K. R. Vogel, T. P. Dinneen, A. Gallagher, and J. L. Hall, Proc. SPIE **3270**, 77 (1998).

[22] Mention of specific product names is strictly for technical communication only.

[23] L. R. Hunter, W. A. Walker, and D. S. Weiss, Phys. Rev. Lett. **56**, 823 (1986).

[24] C. W. Bauschlicher, S. R. Langhoff, and H. Partridge, J. Phys. B **18**, 1523 (1985).